Development of Triboelectric Nanogenerators using Novel 3D Printed Polymer Materials

Muhammad Wajahat[1], Abbas Z. Kouzani[1], Sui Yang Khoo[1], M. A. Parvez Mahmud[2]

[1]School of Engineering, Deakin University, Geelong, VIC 3216, Australia

[2]School of Mathematical and Physical Sciences, University of Technology Sydney, NSW 2007, Australia

Corresponding Author:

Dr M. A. Parvez Mahmud

School of Mathematical and Physical Sciences,

University of Technology Sydney, Australia

Phone: +61 4 2070 7087, E-mail: parvez.mahmud@uts.edu.au

Development of Triboelectric Nanogenerators using Novel 3D Printed Polymer Materials

Abstract— Triboelectric nanogenerators (TENGs) are becoming attractive devices for harvesting mechanical energy. 3D printing (3DP) is a newly reported technique for the development of this device. This technique is not fully explored for fabrication of triboelectric materials and compatible printing processes. In this work, three main 3DP techniques including powder based multi jet fusion (MJF), resin-based poly jet fusion (PJF) and filament based fused deposition modeling (FDM) are utilized to investigate new sets of 3DP triboelectric materials. Mechanical to electrical conversion efficiency of 3D printed and commercially available negative and positive triboelectric materials are compared and investigated. Polyamide 12 (PA12), Veroclear, acrylonitrile styrene acrylate (ASA), copper coated polylactic acid (Cu-PLA), polycarbonate (PC) and polyethylene terephthalate glycol (PETG) are fabricated using compatible 3D printing techniques. In the printing process, the effects of different printing parameters including filling rate, printing temperature and nozzle speed are assessed and optimized. For each material, impacting factors like contact angle, thickness, material profiling and surface texture are also examined. For electrical output characterization, 3D printed PA12 is considered a reference positive triboelectric layer. Meanwhile, 3D printed Veroclear, ASA, Cu-PLA, PC, PETG and commercial materials like Teflon sheets, PA6,6 conductive sheets, indium tin oxide coated polyethylene terephthalate (PET-ITO), conductive nylon sheet and polyvinylidene fluoride (PVDF) membrane are selected as negative triboelectric materials. A power management module is designed to efficiently convert AC output of TENG into DC to power up storage device and LEDs. The maximum open circuit voltage of 80 V and maximum instantaneous current of 0.9 µA is produced by pairing 3DP-PA12 and 3DP-Veroclear. This output is further utilized to efficiently charge up the capacitor and glow series of 16 commercial LEDs lights.

Keywords: 3D printing (3DP), Triboelectric nanogenerators (TENGs), Polyamide 12 (PA 12), Veroclear, Acrylonitrile styrene acrylate (ASA), Material jetting fusion (MJF), Poly jet fusion (PJF), Fused Deposition Modelling (FDM).

1. Introduction

The world is entering in a new generation of Internet of things (IoTs) and self-powered electronics are becoming the building blocks for new industrial revolution [1]. These devices have widespread applications in industrial to personal usages like healthcare, energy-related products, manufacturing activities, smart building technologies, environmental monitoring, and several others [2], [3]. These devices mostly comprise of wearable devices and macrosystems, which need to be designed in a smart manner to be portable and as diminutive as possible. To achieve these features, a smart power supply design is required. Traditionally power supply requirements for these devices are fulfilled by batteries but their size and weight restrict the miniaturization of these devices. Battery replacement issues are critical in distant areas and some extreme environments where wireless sensors are installed. Extreme weather conditions can also lead to power losses and problematic management of high current pulses where battery powered sensors are utilized. Environmental toxicity is another major drawback of using batteries as power source of sensors. Batteries disposal is too complex to be done in an environmentally safe way due to the existence of several toxic chemicals [4]–[6]. To overcome these challenges, it is necessary to design energy generating devices which harvest energy from surrounding environment [7]. Several energy harvesting mechanisms were developed using triboelectric, piezoelectric, thermoelectric, and pyroelectric effect [8]–[12]. Triboelectric nanogenerators (TENGs) are the less complicated structures among all reported energy harvesters. TENGs were invented in 2012 by Zhong Lin Wang [13] and have proved to be an efficient way to convert mechanical forms of energy from surroundings into electricity in sustainable manner [14]–[25]. Self-powered sensors based on TENG exhibit remarkable adaptability in sustainability [26]and proven to be commercially viable in comparison with other energy harvesters [27]. This technology is at the forefront of research and development, and their performance has been demonstrated in several studies done on energy harvesting from mechanical vibration [28], human motion [29], water [30], and air flow [31]. Apart from being a green energy solution, TENGs offer high power output and efficiency, uncomplicated design manufacturing, and ease of material selection, shape adaptive capability and flexibility with low-cost fabrication [13], [32], [33]. The working mechanism of TENG is based on the coupling of triboelectrification and electrostatic induction effect. There are four working modes including contact separation (CS) mode, lateral sliding (LS) mode, Single electrode (SE) mode and freestanding (FS) mode. CS mode generates the charge by vertically separating the two triboelectric materials while LS mode generates the charge by sliding the two triboelectric materials. However, SE mode produces a static charge when freely moving triboelectric material contacts reference electrode attached to the ground. While in FS mode, charges are produced when freely moving triboelectric material contacts with pair of asymmetric electrodes [34]–[36]. In this

study, we have selected contact separation mode after experimenting and compared the results with other operating modes at initial stages.

Several techniques have been deployed till now to fabricate the triboelectric materials at laboratory and commercial scales, which involve several steps of casting, molding, and other assembling stages. Although developing this harvesting device could be done using several traditional manufacturing techniques but these techniques involve complex manufacturing steps and several limitations: size control, poor scalability, slow production rate, commercialization, and restriction of high vacuum system for the fabrication process [37]–[42]. 3D printing is an emerging manufacturing method and has been refined over the last couple of decades. It took over the film-based printing system and is now in vogue for diverse applications. 3D printed electronic sensors [43] , energy-related devices [44], bio-medical applications [45] and several other electronic devices [46] have accelerated this process. Applying 3D printing to create TENGs has so far resulted in several practical benefits, for example, TENG as a complete device is completely compatible with 3D printing unlike electromagnetic generators which require printing of electromagnets and piezoelectric generators. These also require Lanthanide as a dielectric material and high temperature crystallization which 3D printing cannot achieve [47]. In comparison to traditional fabrication techniques, 3DP process results in low energy consumption since 3D printable materials do not require high input power for processing or several post-treatment processes [48]. Most importantly demand of customization of the TENGs structure is fulfilled by precision in patterning of 3D printing [49]. 3D printers can directly print and create digitally optimized surface textures on the triboelectric layers resulting in enhanced overall performance of TENG devices. In recent years, several researchers utilized 3D printing that helped to progress this device by induction into various application on commercial scalee. For instance, 3D printed wearable devices, SOS distress system, LEDs lightening shoes and charging system for smart devices were invented using TENGs by harvesting human motions and converting them into electrical energy. J.P Lee et al.[50] optimized the power output of a fabricated 3DP TENG device and successfully utilized it for charging a smart watch. They also focused on noise cancellation techniques during charging and successfully reduced the noise level by almost 20dB without affecting the output power. In a similar study, Jiang et al. [51] developed a hybrid nanogenerator employing both triboelectric and electromagnetic materials, which produced a contact-free hybrid nanogenerator. It successfully powered up LED lights, sensors, self-powered GPS systems, and mobile phones. 3D-printed triboelectric nanogenerators are employed to recycle sterilized, three-layered surgical masks and nitrile gloves. Under a 9 N force, this device used mechanical motions to generate energy, producing a peak voltage of 50.7 V, a current of 4.8 A, and a power density of 6.39 W/cm^2. This energy was

successfully used to power a variety of small electronics, including wristwatches, digital tally counters, lumex displays, and arrays of 25 interconnected LEDs [52]. In another recent research, surface patterning was used to the layers of the 3DP- TENG to improve output performance. The use of three different pattern geometries circular, linear, and pyramid were studied, and results showed that the pyramid pattern led to a significant increase in output voltage from 80V to 109V in contact separation mode [53].

Although 3D printing has been used by several researchers to refine the development for TENG devices but this technique has not fully been explored due to incompatibility of triboelectric materials and unawareness of printing processes [19], [49], [54]–[61]. In this article, we have investigated, compared, and identified the best performing 3D printed materials which have never been explored previously with reference to TENG. These printable materials are PA12, Veroclear, PETG, PC, CuPLA and ASA. Material analysis was performed to identify these novel materials and already in-practice materials and tested out several combinations for the fabrication and development of TENG. Several properties were considered while selection of material that include compatibility with 3D printing process, electronegativity, tensile strength, flexibility, and impact resistance. Also, dielectric values of these materials were investigated which is a vital property to be considered for TENGs' electrification layer as it affects the electrical output of triboelectric generators [62]. 3DP-PA12 has not have been investigated for the development of TENG device. We selected PA12 polymer as the printing material based on its physicochemical and electrical properties. In a study conducted for PA coating as an electropositive layer, PA functioned better when used as an electropositive layer in TENG [63]. In another study focusing on mechanical properties of 3DP- PA12 revealed that PA12 material can be used as sleeve bearing due to its phenomenal impact resistance strength, tensile strength, and damping properties [64]. A. Salazar et al. [65] analysed stress, strain behaviours and other mechanical properties of printed prototypes in different scenarios. They found that the melting temperature of PA12 is noticeably higher than its crystallization temperature resulting in reduction of stresses and distortions in printed specimens. Based on research reviews, we found that 3D printed PA12 as best compatible and exceptional performer out of all the other polyamides and it also possesses some exceptional mechanical properties in 3D printing which made this a perfect choice for this study. For the negative materials, we utilized 3D printed Veroclear, ASA, Cu-PLA, PC, PETG and several commercial materials like Teflon sheets, PA6,6/Nylon conductive sheets, PET-ITO, and PVDF membrane.

For the printing of polymer materials, three printing techniques are used including PJF using resin-based material, MJF using powder as a printing material and FDM by utilizing polymers filaments. Printing of PA12

is done using MJF, while PJF is utilized to prints a high-quality thin Veroclear film. Whereas, FDM printer is used to print PETG, CuPLA, PC and ASA. 3DP-PA12 is set as a reference positive material and the remaining materials are utilized as negative triboelectric materials. While fabricating TENG, we used two efficient conductive tapes made of Aluminium (Al) and Copper (Cu) as electrodes.

We investigated effects several parameters on the output performance of TENG in this study which include printing parameters, device dimensions (sizes, dielectric layer thickness, gap between materials), dielectric properties and impact of electrode. The complete idea/visuals of TENG materials trials, final material selection of TENG, power management module and an energy storage system are shown in Figure 1. The output performance of TENG of various combinations is assessed by applying open circuit and short circuit conditions. The analysis helps to observe the open circuit voltage and short circuit charge transfer between two triboelectric layers. The maximum open circuit voltage of 80 V and maximum instantaneous current of 0.9 µA are produced by the paired 3DP-PA12 and 3DP-Veroclear. This output is further converted into DC output using an efficient power management module to charge up the capacitor. Storage of the capacitor is then utilized to nearly glow up around 16 commercial LEDs. The comparison analysis and development of these material combinations for triboelectric nanogenerator are unique and can contribute significantly for future refinement of TENG devices. In Section 2, fabricating steps of 3DP-TENG are highlighted, followed by a detailed discussion of the printing process of triboelectric materials, and the material profiling for each material is reported. A detailed discussion on results, significance of current work and future direction are highlighted in section 3.

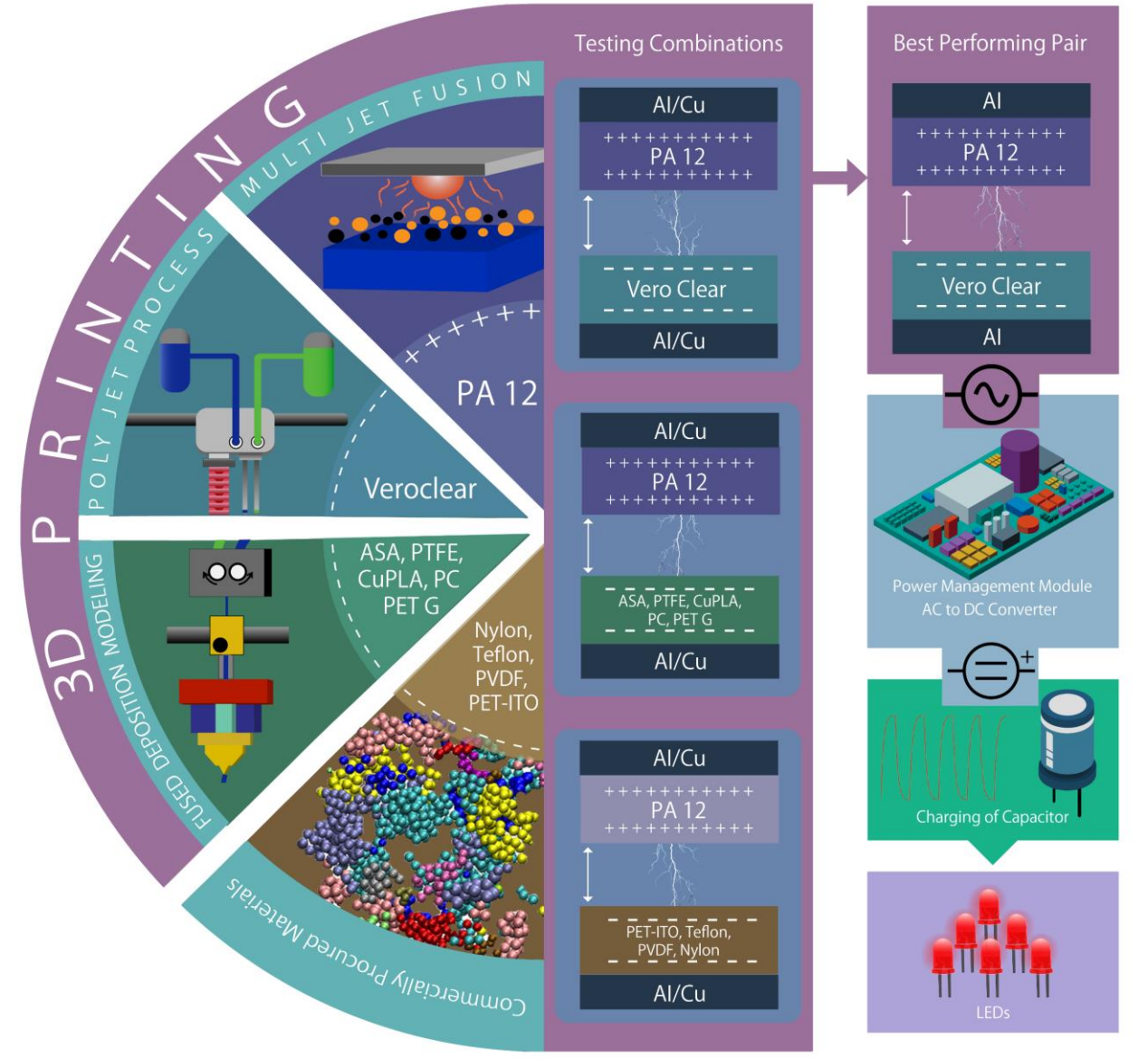

Figure 1 Visuals and working of developed 3DP-TENG, Power management module and its applications

2. Experimental Methodology

In this study, we have developed the triboelectric materials, performed characterization to study the properties of the materials, analyzed the output performance of TENG with several combinations of novel and commercially available materials, selected the best performing combination for power management module and applied load circuit analysis on output power. After careful selection of materials, we applied three different printing techniques for fabrication of TENGs for novel materials that are powder based MJF, Resin based PJF and filament FDM. All these printing processes along with materials are explained in detail in 2.1. Material characterization is performed using FTIR (Fourier Transform infrared) and SEM (Scanning Electron Microscope) analysis. FTIR analysis is performed for all the materials used in this study, however,

SEM is performed for materials which lead to maximum output voltage. This is done to investigate the structural properties and their impact on output performance. This is further explained in section 2.2. Device is assembled in contact-separation mode with two different electrodes that are aluminum and copper. All the pairs are put to test by applying open circuit and short circuit conditions for voltage and current analysis. Combinations giving significant output are shortlisted which are 18 combinations in total. Out of these combinations, best performing pair is selected. Output generated by this pair is further converted into DC output using a power management module, output is utilized into two different applications. Device assembly, measurement analysis and output application are explained in section 2.3. A schematic process diagram for triboelectric material printing using the 3DP process is shown in Figure 2.

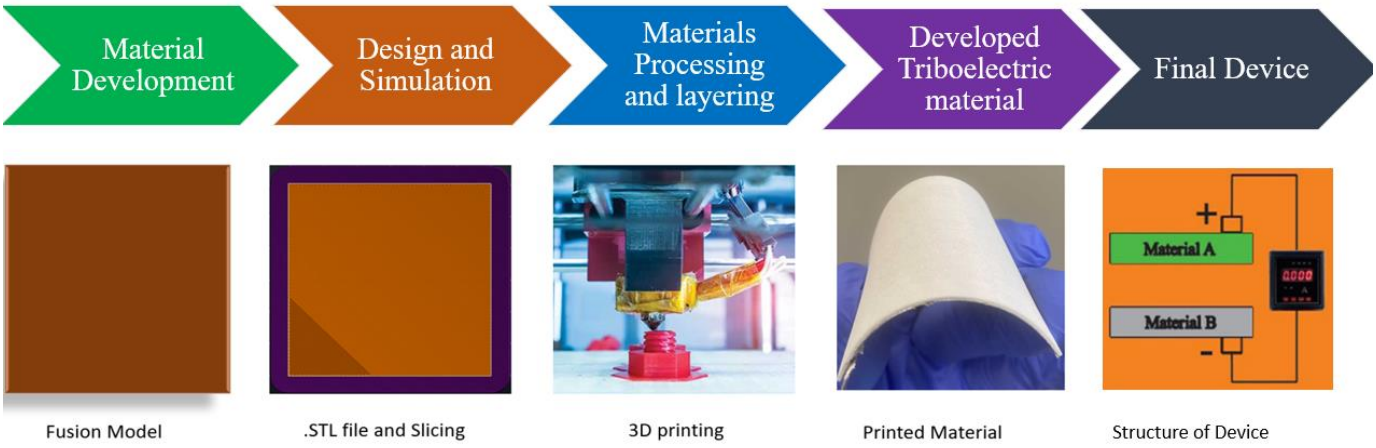

Figure 2: Stages of fabricating 3D printing for TENG

2.1 Printing Methods and Materials Development for TENG

We explored all three types of 3D printing techniques to print the novel materials which includes powder based (MJF), resin based (PJF) and filament based (FDM). Using MJF, we fabricated an electropositive layer of TENG and then we used the rest of the two techniques to prepare different electronegative layers. To create the initial design, a draft 2D drawing of the triboelectric and supporting layer was done using Auto CAD (Computer Aided Design) and Autodesk software. After assessment of the initial 2D design, a 3D model was created using solid work or comparable CAD software. Subsequently, path file in the form of STL were exported for the slicing software of printer. To obtain 2D coordinates for the purpose of layer-by-layer fabrication of triboelectric material, 3D models were further sliced down into 2D using the same slicing software. Model files with .slc extensions (sliced files) were then exported to the printer in the form of

compatible .sml files (Stratasys Machine Language) for further 3D printing processing. To improve the printing process, we used a systematic strategy to the printing settings. Some key impacting parameters, for example nozzle speed, temperature, and the make-up of the support material were carefully adjusted against each material used for printing. We also examined the impact of thickness changes on the triboelectric performance of the printed samples throughout the initial stages of our enquiry. Iterative modifications were made to variables such. We carefully adjusted these parameters through thorough experimentation and analysis to achieve accurate material deposition and ideal interlayer adhesion. A wide range of thicknesses, from 0.1 mm to 0.5 mm, were methodically investigated to determine the ideal thickness that resulted in the greatest charge generation and long-term material stability. Table 1 shows summary of material dimensions and other parameters.

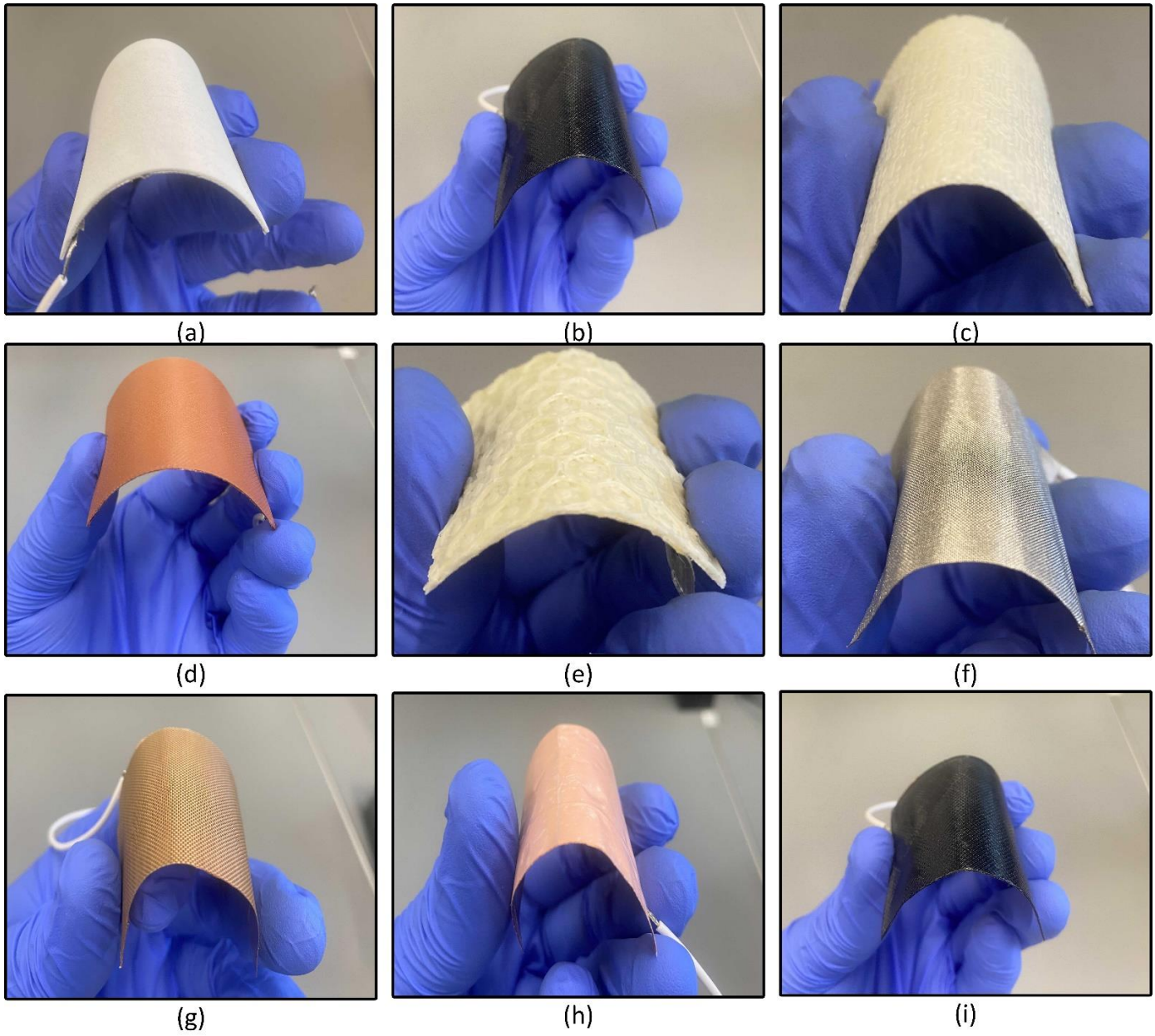

Figure 3:Prepared samples of triboelectric layers (a) PA12 (b) PETG (c) PTFE (d) Cu-PLA (e) Patterned ASA (f) Nylon conductive (g) Teflon sheet (h) Veroclear(i) PC

Table 1: Specifications of prepared samples

Material	Thickness Prepared for Testing (mm)	Thickness Used (mm)	Length (mm)	Width (mm)	Tensile Strength MPa Ex=experimental value DS=value from Data sheet	Printing Parameters			
						Printing Process/Machine	Support material/filament	Nozzle speed mm/s	Nozzle Temp C^0
Polyamide PA12	0.3-0.9	0.4	50	50	47.7 (Ex)	MJF /HP MJF580	HP 3D400	2000-5000	160- 190
Veroclear	0.2-0.9	0.4	50	50	45.2 (Ex)	PJF/ Stratasys Objet500 Connex3	Tango Plus	Auto control	27-35
PC-3DP	0.2-0.5	0.4	50	50	57.9 (DS)	FDM/ Stratasys Fortus 450MC	PVA (polyvinyl alcohol)	20-60	250-300
Cu PLA - 3DP	0.2-0.5	0.3	50	50	45 (DS)		PLA (Polylactic acid)	40-100	180-220
ASA	0.3-0.6	0.3	50	50	32.8 (DS)		SR-30 / 35 (soluble)	40-80	240-270
PETG	0.2-0.6	0.4	50	50	53 (DS)		HIPS (high impact polystyrene)	30-70	210 -235
PTFE/ Teflon	0.3-0.6	0.4	50	50	25-35 (DS)	NA	NA	NA	NA
PTFE thin film	0.3-0.6	0.4	50	50	31.79 (DS)				
PA Conductive	0.3-0.6	0.4	50	50	49.3 (DS)				
PVDF	0.3-0.6	0.4	50	50	43.4 (DS)				
PET-ITO	0.3-0.6	0.4	50	50	52 (DS)				

2.1.1. Printing of Polyamide (PA 12)

We used HP MJF580 printer for printing of PA12 which is used for positive layer of TENG. Steps of this printing technique are shown in Figure 4. For pre-process, .STL files with a thickness ranging from 0.3 to 0.9 mm were prepared. At the first stage of process, PA12 powder was layered down on the printing bed. Powder was used at a ratio of 20:80 (virgin/used) based on the method of Chao. C et al.[66] ,and our specimen size was 50 mm × 50 mm. Once the layering of powder is completed, the MJF head passes across the deposited powder with fusing and detailing agents. In the next stage, the PA12 layer was topped up with fusing and detailing agent which is exposed to ultraviolet rays and enabled the fusing agent to absorb thermal energy and continuously heat up the powder till it reached its melting point, i.e. 187 C˚. Whereas, the detailing agent is evaporated at this stage. This creates a fused layer; the loose powder remains there

and is collected at the post-process stage for reuse purposes. The first printed layer supports the next layer to be printed and this process continues till we obtain our desired layer thickness and shape of TENG as shown in Figure 3(a).

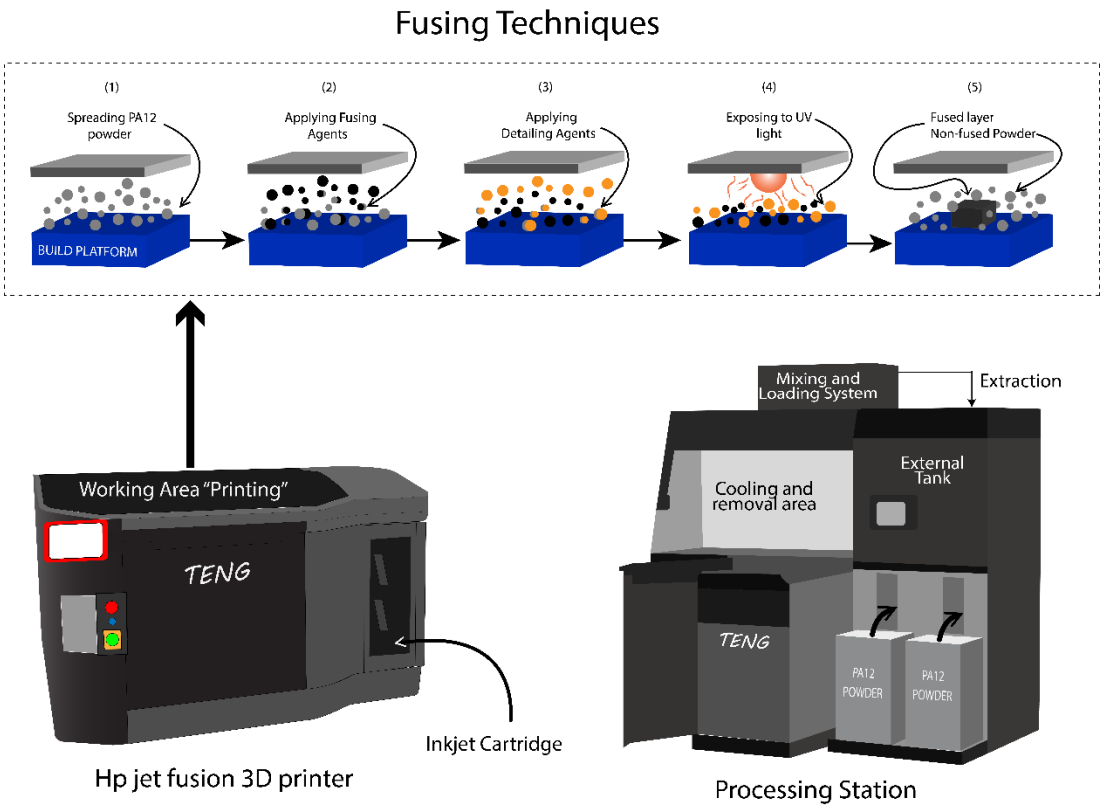

Figure 4: Schematic of Multi Jet Fusion (MJF) process and fusing process steps (1–5)

2.1.2. Printing of Veroclear

To fabricate an electronegative layer of TENG, we used Veroclear as the printing material in polyjet printing method with Stratasys Objet500 Connex3. The idea for using Veroclear came from the fact that it simulates PMMA (Polymethyl Methacrylate) [67], and PMMA has been used as electronegative layer in TENGs [47]. J.C. Santos et al. [68] conducted an experiment by taking PMMA as the reference material for 3D printing of glandular tissues in breast phantom and tried several other polymers including Veroclear as a substitute of PMMA. They found that Veroclear showed reasonable equivalence with PMMA in required properties but until now 3D Veroclear has not been explored for the development of TENG. In addition to this property, Veroclear which has a transparent appearance, showed outstanding tensile strength and impact resistance when used as a polyjet photopolymer. Arivazhagan et al. [69] studied the mechanical properties of printed materials using two different polymers and their effect on the printing process. They compared Veroclear and VeroWhite Plus. They examined the shore hardness, tensile strength, and flexural tests of printed models. Results showed that models with a shiny/glossy finish have greater strength compared to matte

finish models. In another study, Veroclear is used in the field of orthodontics for 3D fabrication of clear aligners. Analysis executed in this study proved that Veroclear performed better in all aspects [70].

Starting from pre-process, a 3D model drawing was created using Fusion 360. This was done to print a thin film of Veroclear resin with different material thicknesses starting from 0.2 to 0.8 mm (50mm × 50 mm), and then the component was positioned on the build platform of the printer as shown in Figure 5. Above that platform, micro jetting heads are placed which spreads the number of photopolymer droplets including Veroclear as a building material while Tango Plus is a support material from a 1200 DPI nozzle on the printing tray. Those droplets are then cured and hardened by ultraviolet light giving strength to the build structure. Jetting and solidification through UV steps are repeated until the whole TENG layer is created. The final process involves removing support material from the build bed manually by using a scraper or spatula, and this was done carefully to avoid any damage to the build bed. Leftovers were cleaned with damp wipes and the nozzle was cleaned by dropping the bed and using a mirror (specifically designed for Stratasys Objet500 Connex3). Post-processing of 3DP- TENG Veroclear layer initially involved cleaning manually, then it was sent to the washing chamber where water jet cleaned the component. As it was a thin layer a high-pressure jet was avoided. It was then soaked in Stratasys NaOH solution for 10 minutes, then cleaned with water and air dried and the final prepared specimen can be seen in Figure 3(h).

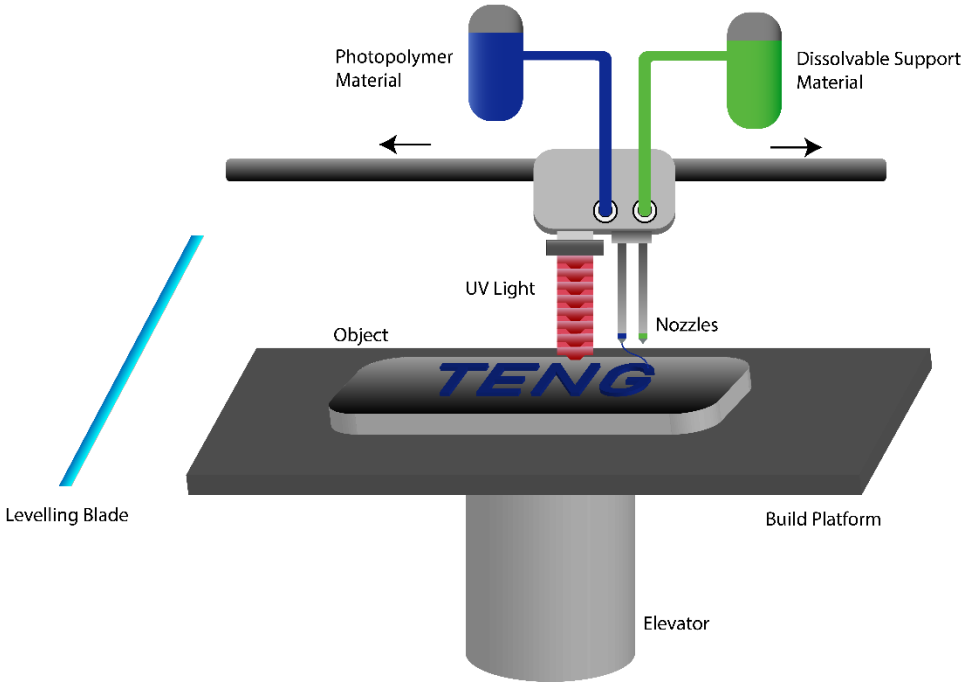

Figure 5: Schematic representation of the material jetting process performed on Objet500 Connex3

2.1.3. Printing of ASA, PTFE, CuPLA, PC and PETG

Based on triboelectric series it can be determined that ASA, PTFE, PETG, PC and PVDF have properties enabling them to function as an electronegative layer in TENGs [71]–[73] . Out of these materials, we printed ASA, PTFE, CuPLA and PETG by using Stratasys Fortus 450MC. 3DP-ASA is like ABS (Acrylonitrile Butadiene Styrene) but with more UV resistance properties due to Acrylate replacing polybutadiene. We have also used a new filament by creating a composite of copper and PLA (Cu-PLA) to investigate its triboelectric properties. A schematic illustration of FDM printing technique using with "Stratasys Fortus 450MC" can be seen in Figure 6. In the first step the FDM layer was printed from the deposition of printing materials in a layer-by-layer form as per the 3D model data (derived from CAD), while FDM printing is primarily based on the process of hot melt extrusion. For ASA, we set the bed temperature of 100°C, while printing/nozzle temperature was 250°C; the support material in this case was SR-30/35 (soluble). Feeding process of FDM is based on filament feedstock and the filament diameter was 2.0 mm. This filament was derived through the mechanism of a circulating gear which gets its energy from the connected stepper motor. To retain the filament and send the feed to the liquefier chamber, significant friction is required and this is achieved by creating grooves/teeth on the drive gears. The exit pressure of the filament from the nozzle is created by a gradient of the melted filament at front end (after passing the heated liquefier) and solid filament at the back end acting as a piston. The prepared samples of ASA, PTFE, CuPLA, and PETG are depicted in Figure 3(b), (c), (d) and (e) respectively.

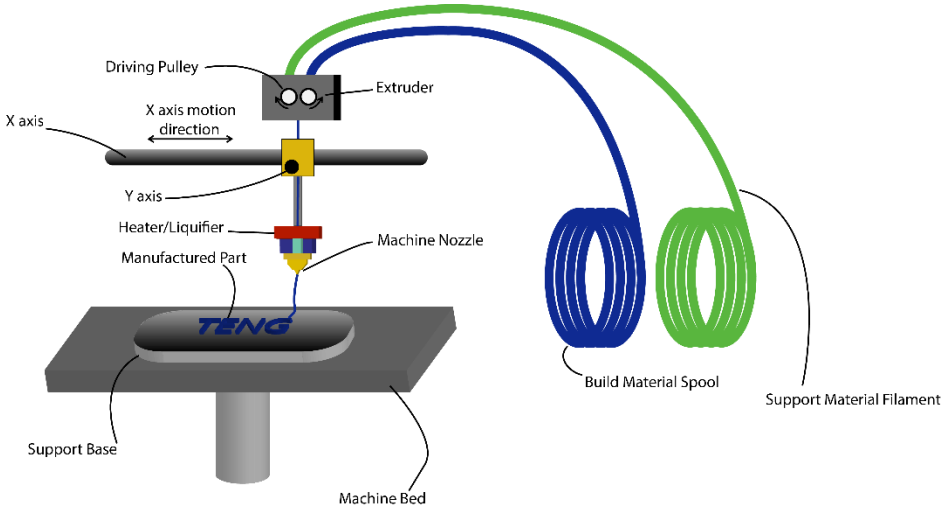

Figure 6: Schematic representation of the FDM printing process

Some other materials used as negative triboelectric layer in testing combinations were procured commercially for example Teflon, PVDF and PET-ITO.

2.2. Materials Characterization

In this study, along with a physical analysis of the sample material, we explored the material's structural and morphological features. This helped to generate information on the material stability and its molecular composition. We selected samples of 3DP PA12, 3DP ASA, Teflon, 3DP cu-PLA, PET-ITO and Veroclear for analysis. To execute the spectroscopic analysis, we used the FTIR technique through VERTEX70 also illustrated in supplementary data video SV1.

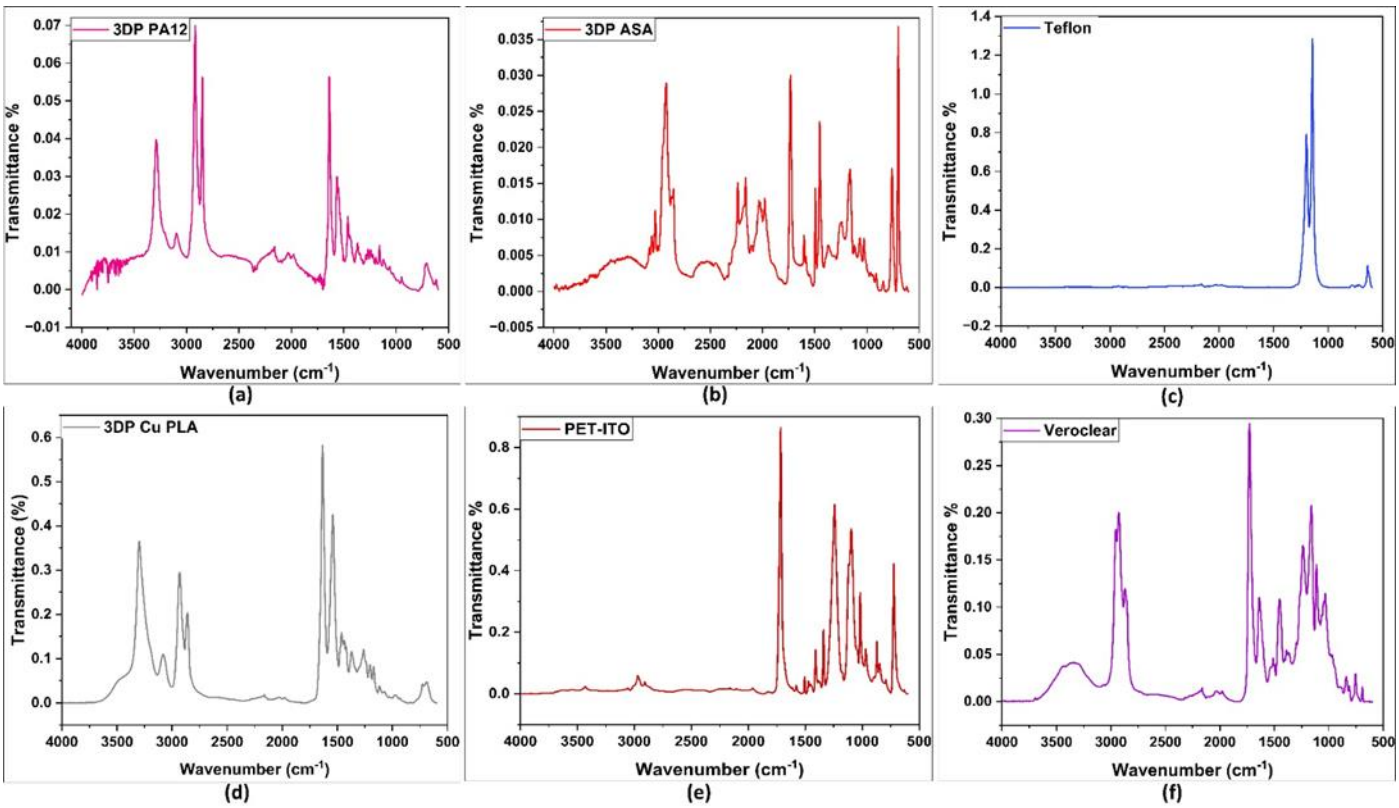

Figure 7: FTIR analysis of Printed Materials used in this study

For each sample, Infrared wavenumbers ranging from 4000 cm-1 to 500 cm-1 were passed (mid IR-spectrum). Each material showed a different behavior of transmittance at applied frequencies. The peaks and drops of transmittance in Figure 7 show the details of chemical bonding. The peaks of Veroclear, PET-ITO and 3DP Cu-PLA are in the same region, i.e. 1720 cm^{-1} wave number which reveals the presence of Acrylate. Peaks of ASA and Teflon are in the fingerprint region while PA12 spiking appears in the single bond region.

SEM analysis of best performing 3D printed triboelectric used in this study is performed by using Joel IT 300 scanning electron microscope shown in supplementary data video SV2. The sample materials are first coated with platinum using LEICA ACE600 sputter coater machine to make the outer surface conductive and ready for SEM analysis which is illustrated in supplementary data video SV3. Figure 8 illustrates SEM images of

PA12 and Veroclear taken at 100 µm and 50 µm to study the overall surface morphology of both materials. Figure 8(a) and (b) revealing the interconnected particles of 3D printed PA12 polymer which is linked with increased surface area for potential charge generation Figure 8(c) and (d) are the showing the smooth texture of Veroclear leading to consistent surface and high charge transfer.

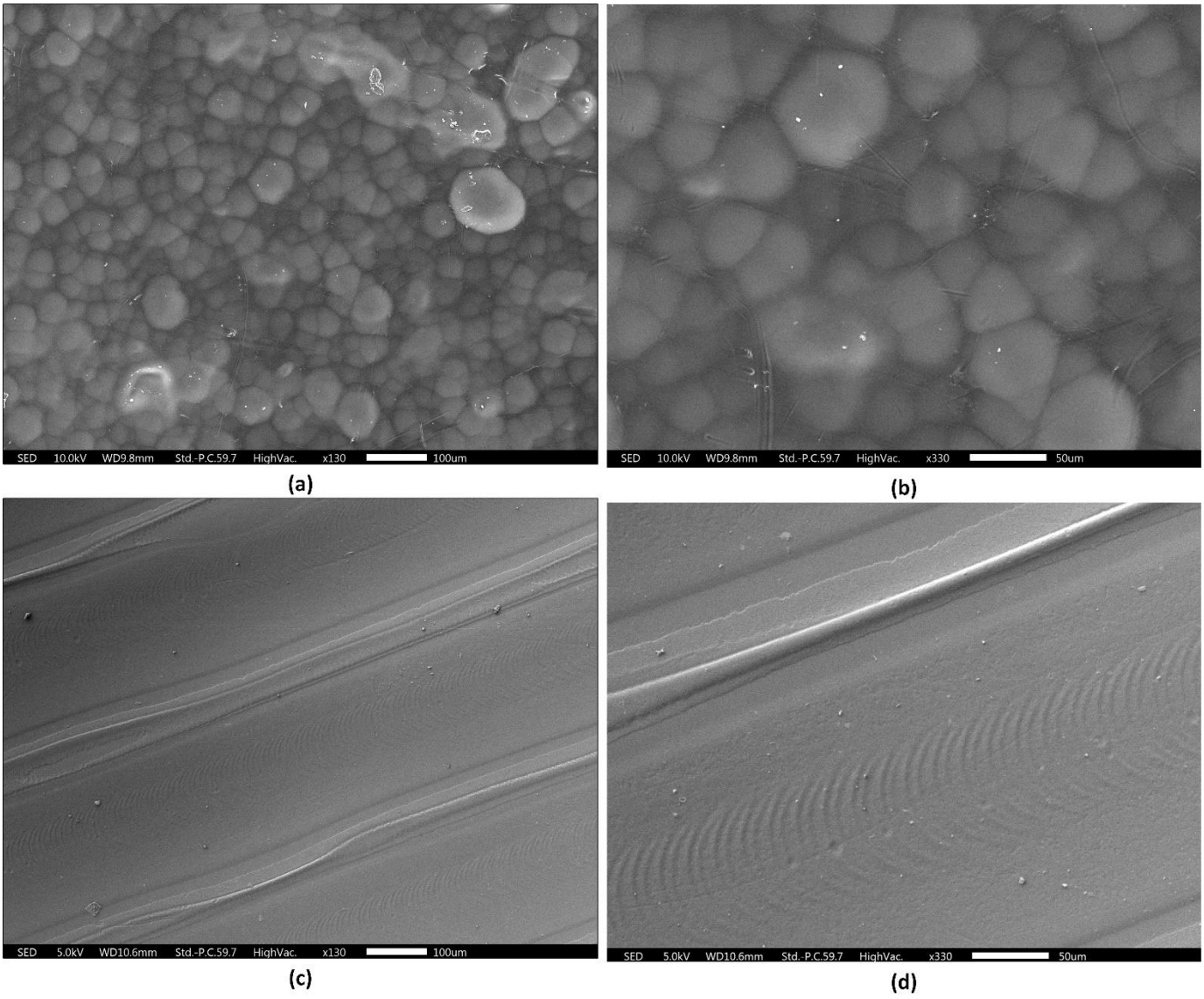

Figure 8: SEM Analysis of PA12 and Veroclear to observe the surface morphology of best performing 3D printed triboelectric materials used in this study (a) SEM visual of 3D printed PA12 at 100 µm (b) SEM visual of 3D printed PA12 at 50 µm (c) SEM visual of 3D printed Veroclear at 100 µm (b) SEM visual of 3D printed Veroclear at 50 µm

To gather the information about mechanical strength and deformation traits, we opted for tensile testing of our samples. We applied controlled axial forces to the selected PA12 and Veroclear specimens using the INSTRON tensile testing device shown in supplementary data video SV4. While the tensile values for other materials were taken from data sheets as our testing focuses on the best performing PA12 and Veroclear. Precision cutting and machining of PA12 and Veroclear specimens were required to obtain a uniform

thickness of 0.4 mm for the tensile testing samples. To ensure uniformity and precision in our examination, these specimens were then aligned in accordance with ASTM D638 standard. The preliminary findings show remarkable tensile strengths, with Veroclear at 52.2 MPa and PA12 measuring 47.6 MPa, graphical analysis of this testing is shown in Figure 9. We baselined the tensile mechanical strength of PA12 from HP data sheet in which PA12 has a tensile strength of 48 MPa and impact strength of 3.5 K J/m2 [74]. Our laboratory results reaffirm the tensile value of PA12. While Stratasys Veroclear data sheet suggests the range of Veroclear tensile strength that is 50-65 Mpa, our results stayed slightly below this range. The results signified the potential of application of these materials in various applications where mechanical integrity is required. This is an additional property of these materials along with other remarkable electrical properties.

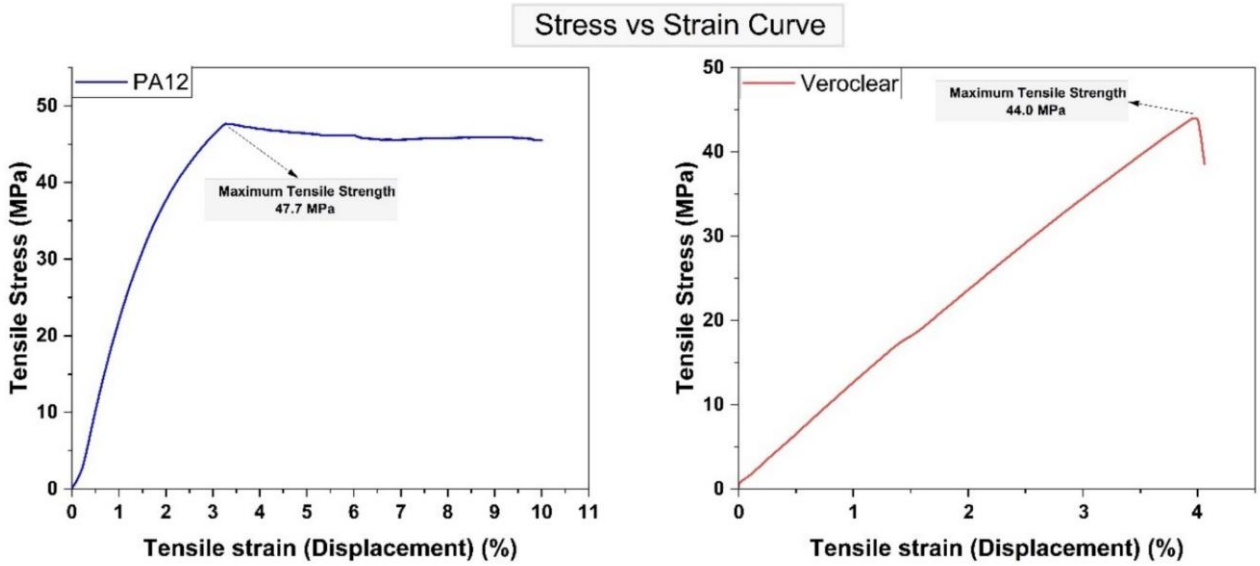

Figure 9: Tensile testing of PA12 and Veroclear

The thickness of each film was measured using Digital Vernier Caliper which can be seen in supporting documents.

In addition to observe the long-term output performance and device reliability of 3DP- PA12- Veroclear TENG. We re-evaluated the device performance after operating the device for several hours over the period of one month using the reported linear motor based experimental setup. Figure 10 is illustrating the surface condition of PA12 and Veroclear after performing this experiment. The device performance was found to be 3.8 % lesser than the output performance recorded at initial stage of the experiment.

Figure 10: Visuals of triboelectric materials post electrical characterization (a) PA12 sample after contact and separation using hand tapping and linear-motor based mechanism (b) Visual of Veroclear after experiment

2.3. Device Assembly, electrical Signal generation, and measurement monitoring

After developing positive and negative triboelectric layers the next stage is to construct a contact separation-based triboelectric device. During the first stage, the electrode layers of Cu and Al have been deposited into the materials. We combined novel 3D printed materials with readily available commercial materials to create a variety of materials for comparison. More than 20 material combinations were created initially. 18 material combinations which resulted in significant power output were shortlisted and reported. After performing mechanical and electrical characterization, we have identified the best performing material and assembled the final device. We used a linear motor-based mechanical-compression system which provides the compression and relaxation force to TENG layers which can be visualized in supplementary data video SV5 and SV6.

2.4. Measurement and monitoring system

An experimental set-up is established to monitor key performance indicators of TENG's output as shown in Figure 11. Open Circuit Voltage (V_{oc}) and short circuit current (I_{sc}) are measured using Oscilloscope, Keithley multimeter and digital multimeter. 12V DC motor is used to perform continuous contact separation between triboelectric materials.

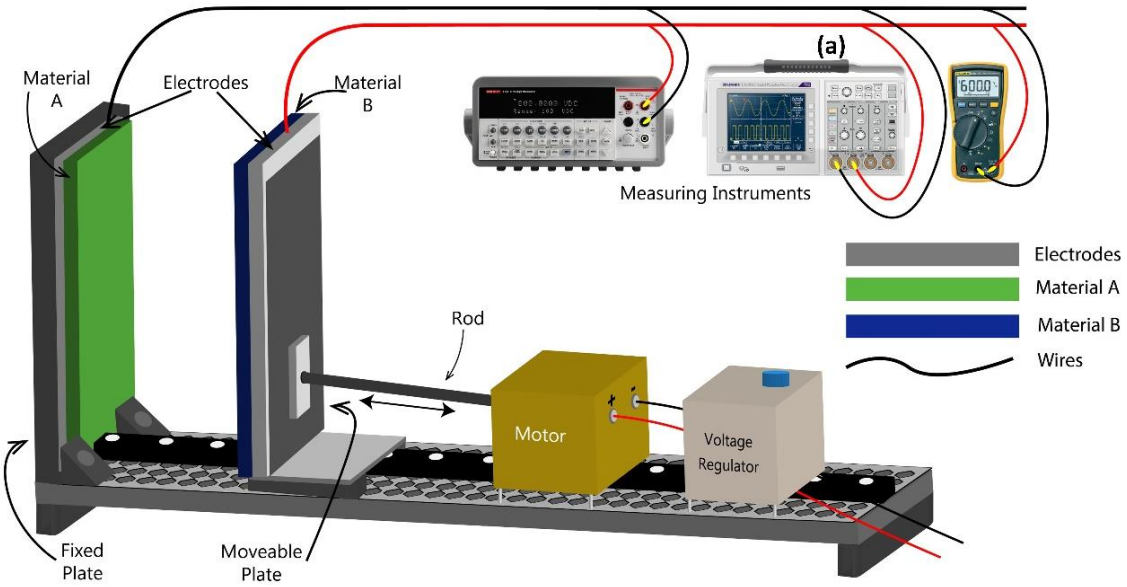

Figure 11: Experimental set-up for contact separation mode 3DP-TENG

3. Results and Discussion

We analyzed the key impacting factors of TENGs. Layer thickness of triboelectric layers, structural properties of these materials and effect on electrical output generation. These factors are discussed in detail in the sections below.

3.1. Electrical Output Performance

Table 2 summarizes the output results of varied materials as electronegative TENG layer with Al and Cu electrodes, respectively. These 18 combinations showed altogether different outputs, and we can see from the results that pairing up PA12 as an electropositive layer and Veroclear as an electronegative layer with Aluminum electrode outperformed all other assemblies. This pair generated maximum power output of 72µW with V_{oc} as high as 81 Volts and generated I_{sc} of 0.9 µ Amperes. In this assembly, effective layer thicknesses of PA12 and Veroclear are 0.4 mm and 0.22 mm and with the geometry of 50 mm × 50 mm respectively.

Table 2: Electrical output results of TENG combinations

Triboelectric Positive Material	Triboelectric Negative Material	Optimum Thickness mm	Geometry (L×W) mm	Max V_{oc} (V)		Max I_{sc} (µA)		Max Power (µW)	
				Al	Cu	Al	Cu	Al	Cu
3DP-Polyamide PA 12 (0.4 mm)	Veroclear -	0.2	50 × 50	81.0	23.4	0.9	0.3	72.6	7.0
	PC-3DP	0.2		55.0	25.0	0.2	0.1	10.9	2.5
	Cu PLA - 3DP	0.2		26.0	11.5	0.1	0.2	2.3	2.0
	PVDF	0.1		65.0	7.0	0.4	0.0	25.8	0.3
	PTFE-3DP	0.2		45.0	10.0	0.8	0.1	35.7	0.7
	PTFE Sheet	0.1		45.0	15.0	0.4	0.1	17.8	1.5
	Nylon	0.1		24.0	13.0	0.5	0.1	11.9	1.8
	ASA- 3DP	0.2		20.0	11.1	0.5	0.9	8.9	10.0
	PET-ITO	0.1		33.0	68.0	0.7	0.1	23.0	7.5

The AC output generated by varied materials paired with PA12 is highlighted in Figure 12. The AC output generated by this pair is then converted to DC output using our designed power management module discussed in above section.

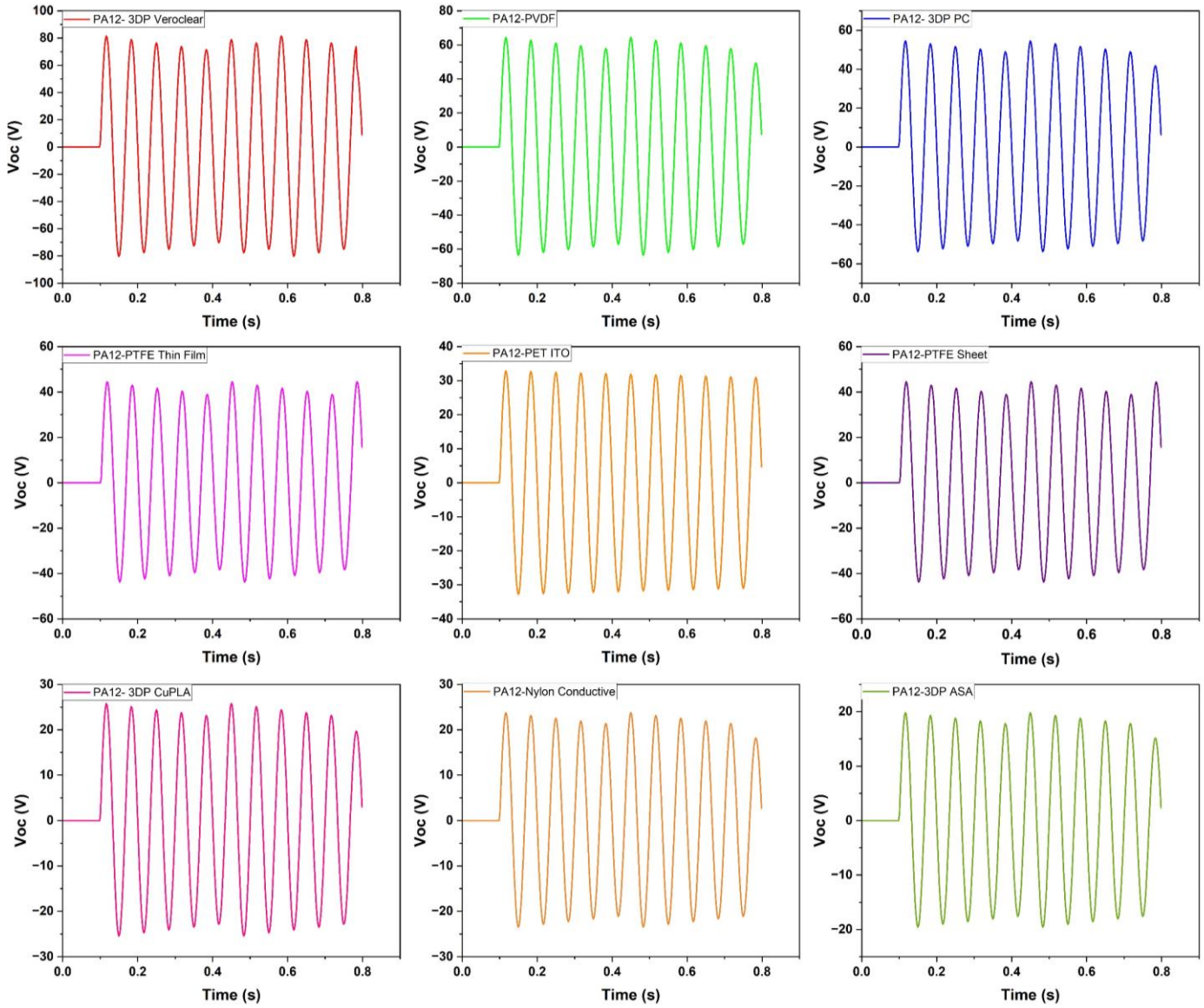

Figure 12: Comparison of AC Output results of different electronegative materials with PA12

There are two types of electrodes being used in this study, copper, and aluminum. Results showed that the pairs with copper electrodes are generating comparatively less output power as compared with aluminum electrodes pair. According to Pauling scale which is proven to be 91% accurate [76]; electronegativity of Aluminum is 0.91 while electronegativity of copper is 1.61. This shows that copper is close to neutral while Aluminum is on positive side of scale. This suggests Al can lose electrons, increasing triboelectric charge generation efficiency. To The comparison analysis of DC output by using Cu/ Al electrode with varied materials combination, when PA12 is fixed electropositive material is shown Figure 13.

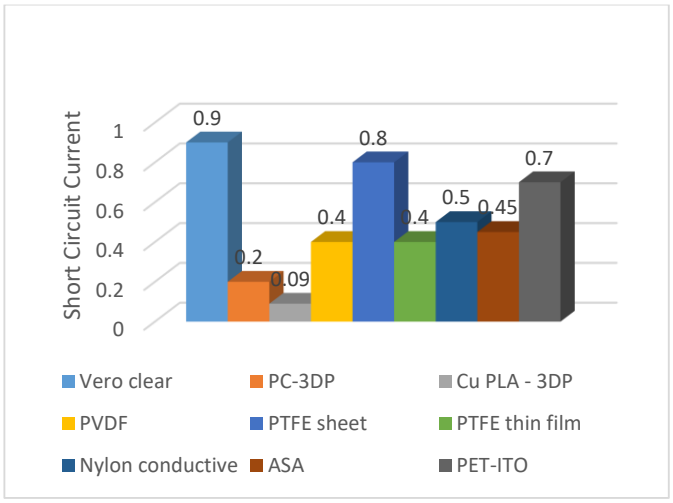

(a)

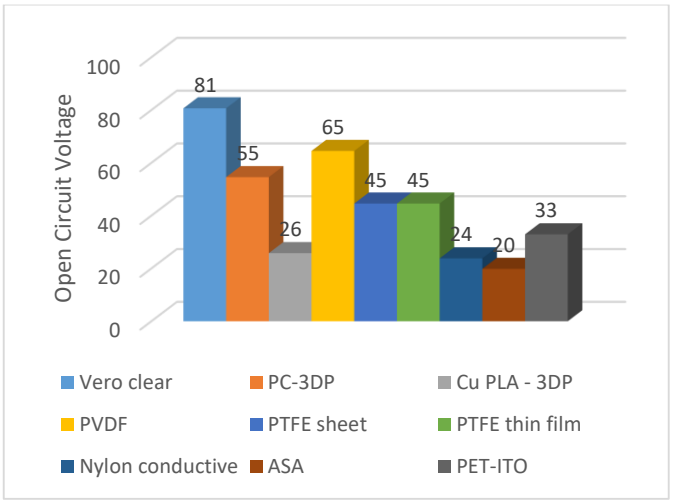

(b)

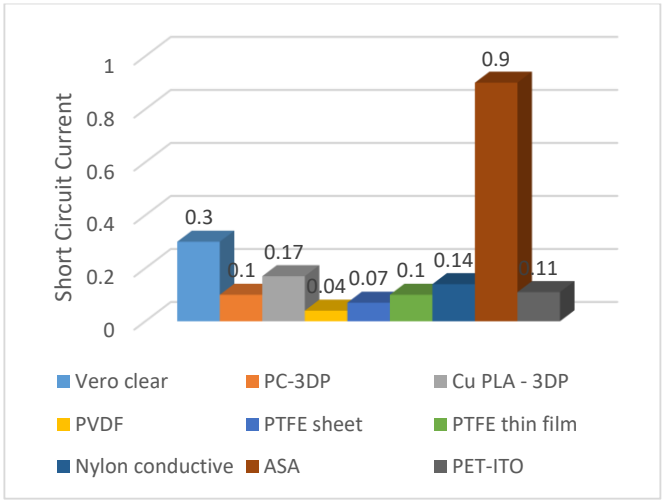

(c)

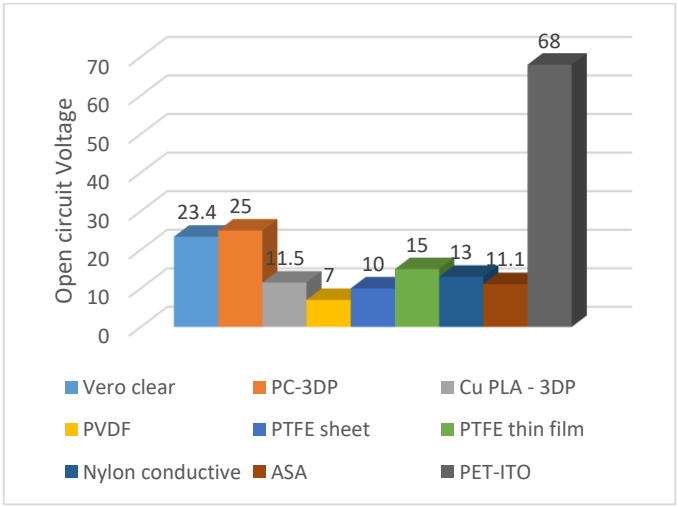

(d)

Figure 13: (a) Comparison of short circuit current of different electronegative with 3DP-PA12 electropositive TENG layer using Al as the electrode (b) Comparison of open circuit voltage of different electronegative with 3DP-PA12 electropositive TENG layer using layer using Al as the electrode: (c) Comparison of short circuit current of different electronegative with 3DP-PA12 electropositive TENG layer using Cu as the electrode (d) Comparison of open circuit voltage of different electronegative with 3DP-PA12 electropositive TENG layer using layer using Cu as the electrode

We have taken the highest performing 3DP- PA12- Veroclear pair to observe the output behavior while applying the load condition. This analysis is performed by adding load resistance from 1kΩ-10kΩ in parallel with capacitive circuit. The voltage drop is then calculated across the resistors to understand the behavior of the circuit. It is observed that voltage drop is increased from 2.269 V to 4.852 V when the load resistance is increased from 1kΩ to 10 kΩ. Figure 14 shows the trend of voltage drop and output power reduction by applying the resistances.

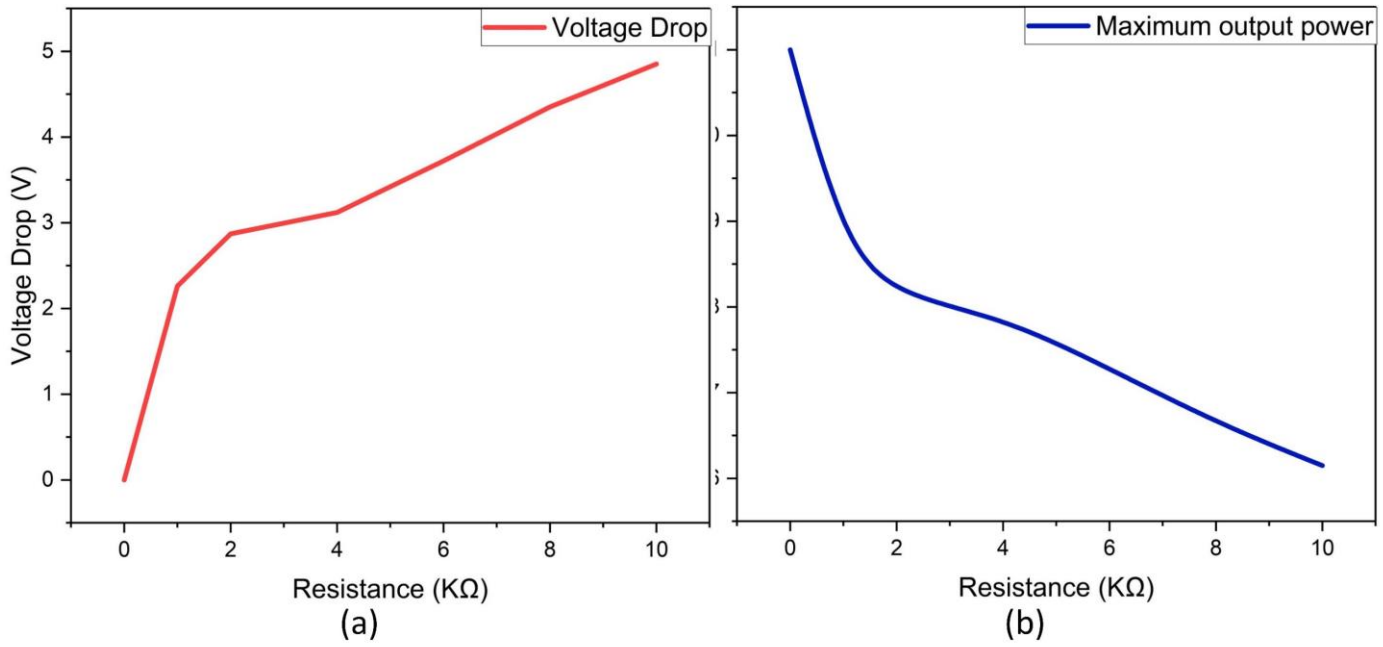

Figure 14: (a) Resistance vs voltage drop (b) Resistance vs maximum outut voltage

3.2. Layer thickness of TENG materials

As thickness of dielectric layers (electropositive and negative layers) significantly impacts the output efficiency. We printed the layers with variable thicknesses. Effect of layer thickness was firstly analyzed on physical characteristic. Optimum thickness on which the material withstood applied force was utilized for further experimenting. Secondly, we measured V_{oc} and I_{sc} at various thicknesses. For electropositive layer of PA12, we printed layers of thickness ranging from 0.3 to 0.9 mm. PA12 is powder-based so at 0.3 mm, PA12 did not withstand external force, also the structure at this thickness was brittle. Optimum thickness of PA12 was found to be 0.4 mm. Veroclear (Electronegative layer) was printed with a variable thickness of 0.2 to 0.6. The best performance was found at 0.2mm. Results of electrical outputs at variable thickness of PA12 and Veroclear are summarized in Table 3. Beyond minimum thickness mentioned in this table, material did not withstand external force and was unstable. Furthermore, it is evident from the results that by increasing thickness of layer, electrical output decreases significantly.

Table 3: Electrical results at various thickness

3DP PA12 Thickness (mm)	Veroclear Thickness (mm)	Max V_{oc} (V)	Max I_{sc} (µA)	Max Power (µW)
0.4	0.2	81.0	0.9	72.6
0.5		72	0.8	57.6
0.6		27	0.4	10.8
0.7		11	-	-
0.8		11	-	-
0.9		3	-	-
	0.3	65	0.67	43.55
	0.4	44	0.41	18.04

0.4	0.5	14	-	-
	0.6	5	-	-

Similarly, the rest of the materials were printed in different ranges and the best performing layer thickness in assembling the TENG combinations mentioned in Table 2.

3.3. Chemical structural impact of PA12 and Veroclear

According to FTIR analysis, Veroclear showed peaks in π- bond region and highlighted the presence of Acrylate. π- bonds have high polarity as compared to sigma bonds which leads to increased dipole moment and enhanced charge transfer between TENG layers and increased electrical output. Another distinguished factor of Veroclear performance is its chemical composition. As, studies showed that ester group has high polarity which results in increased TENG output [77]. Li Wang et al. undertook a structural analysis of Veroclear and found that the major component in its structure is Isobornyl-acrylate (IBOA) which constituted 51% of its composition. Its molecular formula is $C_{13}H_{20}O_2$ and Veroclear 's major component IBOA showed that it has exposed and un-hindered ester group (C=O) contributing mostly to polarity enhancement of Veroclear. Furthermore, the structure of IBOA has a huge similarity with aromatic ring and in one study, the aromatic polymer films increased both the charge-traps and TENG output [78]. Apart from electrical output efficiency, Veroclear produced a clear transparent, high stress/ the impact resistance and highly elastic (less brittle) layer of TENG which were add-ons and encouraged its repetitive usage. The FTIR analysis shows distinct absorption peaks indicate high degree of crystallinity. This is associated with high mechanical strength and thermal stability when used for TENGs application.

On the other side, the ability of PA12 to give or accept electrons during contact electrification in TENGs is influenced by the presence of polar amide groups and the overall molecular structure of the material. The amide groups in PA12 are polar, which aids in the polymer's capacity to create hydrogen bonds between polymer chains, improving its mechanical and thermal durability.[79], [80] .

3.4. Power conversion and storage

An efficient power management system is core requirement for enhancement of TENGs functioning [75]. Our power management module is designed based on the required rating of bridge rectifier, where two diodes conduct the positive sinusoidal wave while the other two conduct the negative sinusoidal signal. The 3D printed TENG worked as an energy harvester which converts the ambient energy into AC signal which is then sent to our power management module. The bridge rectifier circuitry that converts the AC input to DC output is highlighted in Figure 15 (b). The 100µF, 63VDC and low ESR electrolytic capacitor is utilized as a storage device. This can be seen in capacitor charging curve shown in Figure 15 (c). The capacitor output is then utilized to store the DC output coming from the power management module to get around 16 low

voltage commercial LEDs to glow at a rating of 6 mcd/3 mm, illustrated in Figure 15(a).

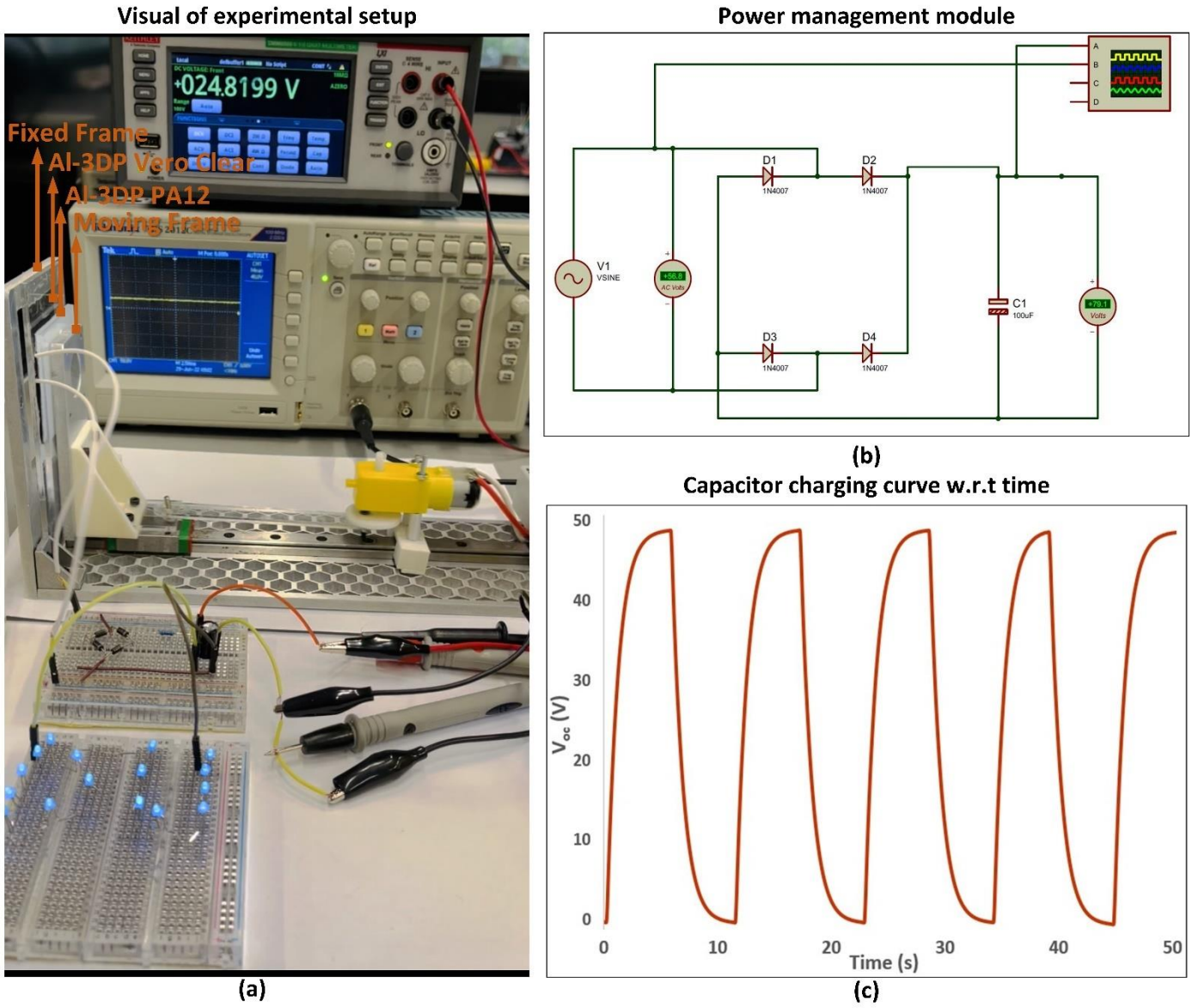

Figure 15: (a) Illustration of Final device assembly and glowing lights, experimental setup and glowing lights (b) Rectifier circuitry design for AC to DC conversion (c) Charging behavior of Capacitor w.r.t time

Aiming to develop a 3D printed triboelectric nanogenerator, this study can be useful to generate electrical energy to charge up storage devices. Conventionally, TENG layers fabrication involves intricate steps of casting, molding, assembling and post-treatment processes; developing TENG devices with 3D printing has numerous benefits including fast prototyping, customized design freedom and ease of operation. Our study reports a well explained analysis of options available for 3D printable material used for TENG fabrication. This technique will help to replace and digitalize traditional manufacturing methods. Several studies have

utilized 3DP for the development of TENGs but none have performed a detailed analysis of different printing techniques which can be used for devising triboelectric materials [39], [47], [81], [82]. Also, they have explored and investigated only limited materials combinations and ignored the key printing parameters affecting the output performance of TENG [61], [83]–[85]. Herein, we investigated material compositions, layer thickness, layer combinations, options of electrodes, printing techniques and several other parameters. We proposed new materials for this purpose and detected differentiated behaviors of these novel materials. This gives a new dimension to sustainable energy harvesting technique of TENG by simplifying the fabrication process and providing many more options to be explored.

4. CONCLUSION

The potential of novel 3D printed (3DP) material combinations for the advancement of triboelectric nanogenerators (TENGs) is carefully studied and assessed in this extensive study. 3DP printing based on MJF, PJF and FDM is fully demonstrated in this study and optimization of several printing parameters is performed, including material selection, printing temperature, and nozzle speed. To get the best output results, we investigated a wide range of innovative material combinations. We evaluated more than 50 different pairings of triboelectric materials. This included 3D printed and commercially available materials, considering aspects like thickness, material composition, texture, and other mechanical properties. We have highlighted the 18 most effective pairings from our thorough investigation. Further testing revealed that the combination of 3DP-PA12 and 3DP-VeroClear produced a maximum open circuit voltage of 81 V and a peak instantaneous current of 0.9 A. We successfully converted the AC output to DC using a power management module, which was then used to charge a 100 µF, 63VDC capacitor to glow up 16 commercial LEDs with a 6 mcd/3mm rating. This innovative outcome has enormous potential for the development of self-powered systems and a wide range of wearable electronic applications on an industrial scale, in addition to providing essential insights for researchers exploring 3D printing techniques for TENG devices.

CREDIT AUTHOR STATEMENT

Muhammad Wajahat: Conceptualization, Methodology, Lab experimental work, Writing – original draft.

Abbas Z. Kouzani: Supervision, Conceptualization, Writing – review & editing

Sui Yang Khoo: Supervision, Conceptualization, Writing – review & editing

M. A. Parvez Mahmud: Supervision, Conceptualization Writing – review & editing

DECLARATION OF INTERESTS

The authors declare that they have no known competing financial interests or personal relationships that could have appeared to influence the work reported in this paper.

FUNDING AND ACKNOWLEDGMENT

This work is supported and funded by Deakin University Postgraduate Research Program (DUPRS). We would like to acknowledge Saima Hassan for her support in material's conductive coating for SEM analysis.

REFERENCES

[1] G. Yao *et al.*, "Bioinspired triboelectric nanogenerators as self-powered electronic skin for robotic tactile sensing," *Wiley Online LibraryG Yao, L Xu, X Cheng, Y Li, X Huang, W Guo, S Liu, ZL Wang, H WuAdvanced Functional Materials, 2020•Wiley Online Library*, vol. 30, no. 6, Feb. 2019, doi: 10.1002/adfm.201907312.

[2] M. Zhu *et al.*, "Haptic-feedback smart glove as a creative human-machine interface (HMI) for virtual/augmented reality applications," *Sci Adv*, vol. 6, no. 19, May 2020, doi: 10.1126/SCIADV.AAZ8693.

[3] L. Zhou *et al.*, "Rationally Designed Dual-Mode Triboelectric Nanogenerator for Harvesting Mechanical Energy by Both Electrostatic Induction and Dielectric Breakdown Effects," *Adv Energy Mater*, vol. 10, no. 24, p. 2000965, Jun. 2020, doi: 10.1002/AENM.202000965.

[4] Z. L. Wang, "Triboelectric Nanogenerator (TENG)—Sparking an Energy and Sensor Revolution," *Adv Energy Mater*, vol. 10, no. 17, p. 2000137, May 2020, doi: 10.1002/AENM.202000137.

[5] A. Dionisi, D. Marioli, E. Sardini, and M. Serpelloni, "Autonomous Wearable System for Vital Signs Measurement With Energy-Harvesting Module," *IEEE Trans Instrum Meas*, vol. 65, no. 6, pp. 1423–1434, Jun. 2016, doi: 10.1109/TIM.2016.2519779.

[6] S. Ma *et al.*, "Temperature effect and thermal impact in lithium-ion batteries: A review," *Progress in Natural Science: Materials International*, vol. 28, no. 6, pp. 653–666, Dec. 2018, doi: 10.1016/J.PNSC.2018.11.002.

[7] L. Dhakar, F. E. H. Tay, and C. Lee, "Investigation of contact electrification based broadband energy harvesting mechanism using elastic PDMS microstructures," *Journal of Micromechanics and Microengineering*, vol. 24, no. 10, p. 104002, Sep. 2014, doi: 10.1088/0960-1317/24/10/104002.

[8] J. Wu, Y. Zheng, and X. Li, "Recent progress in self-powered sensors based on triboelectric nanogenerators," *Sensors*, vol. 21, no. 21. MDPI, Nov. 01, 2021. doi: 10.3390/s21217129.

[9] Y. Yang *et al.*, "Flexible pyroelectric nanogenerators using a composite structure of lead-free KNbO3 nanowires," *Advanced Materials*, vol. 24, no. 39, pp. 5357–5362, Oct. 2012, doi: 10.1002/adma.201201414.

[10] Y. Yang, Z. H. Lin, T. Hou, F. Zhang, and Z. L. Wang, "Nanowire-composite based flexible thermoelectric nanogenerators and self-powered temperature sensors," *Nano Res*, vol. 5, no. 12, pp. 888–895, 2012, doi: 10.1007/s12274-012-0272-8.

[11] Z. L. Wang, G. Zhu, Y. Yang, S. Wang, and C. Pan, "Progress in nanogenerators for portable electronics," *Materials Today*, vol. 15, no. 12, pp. 532–543, Dec. 2012, doi: 10.1016/S1369-7021(13)70011-7.

[12] S. Niu and Z. L. Wang, "Theoretical systems of triboelectric nanogenerators," *Nano Energy*, vol. 14, pp. 161–192, May 2015, doi: 10.1016/j.nanoen.2014.11.034.

[13] J. Zhu *et al.*, "Progress in TENG technology—A journey from energy harvesting to nanoenergy and nanosystem," *EcoMat*, vol. 2, no. 4, p. e12058, Dec. 2020, doi: 10.1002/EOM2.12058.

[14] Y. Pang *et al.*, "Tribotronic Enhanced Photoresponsivity of a MoS2 Phototransistor," *Wiley Online Library*, vol. 3, no. 6, Jan. 2016, doi: 10.1002/advs.201500419.

[15] X. Gao *et al.*, "A turbine disk-type triboelectric nanogenerator for wind energy harvesting and self-powered wildfire pre-warning," *Mater Today Energy*, vol. 22, p. 100867, Dec. 2021, doi: 10.1016/j.mtener.2021.100867.

[16] M. Wu *et al.*, "Thin, soft, skin-integrated foam-based triboelectric nanogenerators for tactile sensing and energy harvesting," *Mater Today Energy*, vol. 20, p. 100657, Jun. 2021, doi: 10.1016/j.mtener.2021.100657.

[17] M. Sahu, S. Hajra, J. Bijelic, D. Oh, I. Djerdj, and H. J. Kim, "Triple perovskite-based triboelectric nanogenerator: a facile method of energy harvesting and self-powered information generator," *Mater Today Energy*, vol. 20, p. 100639, Jun. 2021, doi: 10.1016/j.mtener.2021.100639.

[18] Y. Liu, G. Liu, T. Bu, and C. Zhang, "Effects of interfacial acid–base on the performance of contact–separation mode triboelectric nanogenerator," *Mater Today Energy*, vol. 20, p. 100686, Jun. 2021, doi: 10.1016/j.mtener.2021.100686.

[19] H. Li *et al.*, "All-printed soft triboelectric nanogenerator for energy harvesting and tactile sensing," *Nano Energy*, vol. 78, p. 105288, Dec. 2020, doi: 10.1016/j.nanoen.2020.105288.
[20] J. Shao, T. Jiang, and Z. Wang, "Theoretical foundations of triboelectric nanogenerators (TENGs)," *Sci China Technol Sci*, vol. 63, no. 7, pp. 1087–1109, Jul. 2020, doi: 10.1007/s11431-020-1604-9.
[21] Z. L. Wang, "On the expanded Maxwell's equations for moving charged media system – General theory, mathematical solutions and applications in TENG," *Materials Today*, vol. 52, pp. 348–363, Jan. 2022, doi: 10.1016/j.mattod.2021.10.027.
[22] J. Luo and Z. L. Wang, "Recent progress of triboelectric nanogenerators: From fundamental theory to practical applications," *EcoMat*, vol. 2, no. 4, Dec. 2020, doi: 10.1002/eom2.12059.
[23] C. Liu *et al.*, "A wind-driven rotational direct current triboelectric nanogenerator for self-powered inactivation of seawater microorganisms," *Mater Today Energy*, vol. 26, p. 100991, Jun. 2022, doi: 10.1016/j.mtener.2022.100991.
[24] H. Dang *et al.*, "Triboelectric-electromagnetic hybrid generator with the inertia-driven conversion mechanism for wind energy harvesting and scale warning," *Mater Today Energy*, vol. 29, p. 101136, Oct. 2022, doi: 10. 1080/ 19392 699. 2020. 17278 96.
[25] Y. Fan *et al.*, "Negative triboelectric polymers with ultrahigh charge density induced by ion implantation," *Nano Energy*, vol. 90, Dec. 2021, doi: 10.1016/j.nanoen.2021.106574.
[26] J. Wu, Y. Zheng, and X. Li, "Recent progress in self-powered sensors based on triboelectric nanogenerators," *Sensors*, vol. 21, no. 21. MDPI, Nov. 01, 2021. doi: 10.3390/s21217129.
[27] P. Munirathinam *et al.*, "A comprehensive review on triboelectric nanogenerators based on Real-Time applications in energy harvesting and Self-Powered sensing," *Materials Science and Engineering: B*, vol. 297, Nov. 2023, doi: 10.1016/j.mseb.2023.116762.
[28] M. Ma *et al.*, "Development, applications, and future directions of triboelectric nanogenerators," *Nano Res*, vol. 11, no. 6, pp. 2951–2969, Jun. 2018, doi: 10.1007/s12274-018-1997-9.
[29] M. Renaud, P. Fiorini, R. Van Schaijk, and C. Van Hoof, "Harvesting energy from the motion of human limbs: the design and analysis of an impact-based piezoelectric generator," *Smart Mater Struct*, vol. 18, no. 3, p. 035001, Jan. 2009, doi: 10.1088/0964-1726/18/3/035001.
[30] Z. Wang, T. Jiang, L. X.-N. Energy, and undefined 2017, "Toward the blue energy dream by triboelectric nanogenerator networks," *Elsevier*, 2017, doi: 10.1016/j.nanoen.2017.06.035.
[31] Z. L. Wang, L. Lin, J. Chen, S. Niu, and Y. Zi, "Triboelectric Nanogenerator: Freestanding Triboelectric-Layer Mode," pp. 109–153, 2016, doi: 10.1007/978-3-319-40039-6_5.
[32] Y. Yu, Z. Li, Y. Wang, S. Gong, and X. Wang, "Sequential Infiltration Synthesis of Doped Polymer Films with Tunable Electrical Properties for Efficient Triboelectric Nanogenerator Development," *Advanced Materials*, vol. 27, no. 33, pp. 4938–4944, Sep. 2015, doi: 10.1002/ADMA.201502546.
[33] Y. Zi *et al.*, "An inductor-free auto-power-management design built-in triboelectric nanogenerators," *Nano Energy*, vol. 31, pp. 302–310, Jan. 2017, doi: 10.1016/J.NANOEN.2016.11.025.
[34] R. Walden, I. Aazem, A. Babu, and S. C. Pillai, "Textile-Triboelectric nanogenerators (T-TENGs) for wearable energy harvesting devices," *Chemical Engineering Journal*, vol. 451. Elsevier B.V., Jan. 01, 2023. doi: 10.1016/j.cej.2022.138741.
[35] C. Wu, A. C. Wang, W. Ding, H. Guo, and Z. L. Wang, "Triboelectric Nanogenerator: A Foundation of the Energy for the New Era," *Adv Energy Mater*, vol. 9, no. 1, p. 1802906, Jan. 2019, doi: 10.1002/aenm.201802906.
[36] C. Xu *et al.*, "On the Electron-Transfer Mechanism in the Contact-Electrification Effect," *Advanced Materials*, vol. 30, no. 15, Apr. 2018, doi: 10.1002/adma.201706790.
[37] M. L. Seol, J. W. Han, D. Il Moon, K. J. Yoon, C. S. Hwang, and M. Meyyappan, "All-printed triboelectric nanogenerator," *Nano Energy*, vol. 44, pp. 82–88, Feb. 2018, doi: 10.1016/J.NANOEN.2017.11.067.
[38] D. Jiang *et al.*, "A wearable noncontact free-rotating hybrid nanogenerator for self-powered electronics," *InfoMat*, vol. 2, no. 6, pp. 1191–1200, Nov. 2020, doi: 10.1002/inf2.12103.
[39] B. Chen *et al.*, "Three-dimensional ultraflexible triboelectric nanogenerator made by 3D printing," *Nano Energy*, vol. 45, no. December 2017, pp. 380–389, 2018, doi: 10.1016/j.nanoen.2017.12.049.
[40] M. Tian *et al.*, "Engineering flexible 3D printed triboelectric nanogenerator to self-power electro-Fenton degradation of pollutants," *Nano Energy*, vol. 74, p. 104908, Aug. 2020, doi: 10.1016/j.nanoen.2020.104908.
[41] H. J. Yoon *et al.*, "3D-printed biomimetic-villus structure with maximized surface area for triboelectric nanogenerator and dust filter," *Nano Energy*, vol. 63, no. April, p. 103857, 2019, doi: 10.1016/j.nanoen.2019.103857.
[42] H. Li *et al.*, "3D printed flexible triboelectric nanogenerator with viscoelastic inks for mechanical energy harvesting," *Nano Energy*, vol. 58, pp. 447–454, Apr. 2019, doi: 10.1016/J.NANOEN.2019.01.066.
[43] J. W. Han, B. Kim, J. Li, and M. Meyyappan, "Carbon nanotube based humidity sensor on cellulose paper," *Journal of Physical Chemistry C*, vol. 116, no. 41, pp. 22094–22097, Oct. 2012, doi: 10.1021/JP3080223/ASSET/IMAGES/MEDIUM/JP-2012-080223_0005.GIF.
[44] N. Han, D. Zhao, J. U. Schluter, E. S. Goh, H. Zhao, and X. Jin, "Performance evaluation of 3D printed miniature electromagnetic energy harvesters driven by air flow," *Appl Energy*, vol. 178, pp. 672–680, Sep. 2016, doi: 10.1016/J.APENERGY.2016.06.103.

[45] B. C. Gross, J. L. Erkal, S. Y. Lockwood, C. Chen, and D. M. Spence, “Evaluation of 3D Printing and Its Potential Impact on Biotechnology and the Chemical Sciences,” *Anal Chem*, vol. 86, no. 7, pp. 3240–3253, Apr. 2014, doi: 10.1021/ac403397r.

[46] J. Yang, M. K. Choi, D. Kim, and T. Hyeon, “Designed Assembly and Integration of Colloidal Nanocrystals for Device Applications,” *Advanced Materials*, vol. 28, no. 6, pp. 1176–1207, Feb. 2016, doi: 10.1002/adma.201502851.

[47] N. Divakaran, J. P. Das, A. K. P V, S. Mohanty, A. Ramadoss, and S. K. Nayak, “Comprehensive review on various additive manufacturing techniques and its implementation in electronic devices,” *J Manuf Syst*, vol. 62, pp. 477–502, Jan. 2022, doi: 10.1016/j.jmsy.2022.01.002.

[48] M. Wajahat, A. Z. Kouzani, S. Y. Khoo, and M. A. P. Mahmud, “A review on extrusion-based 3D-printed nanogenerators for energy harvesting,” *Journal of Materials Science*, vol. 57, no. 1. Springer, pp. 140–169, Jan. 01, 2022. doi: 10.1007/s10853-021-06637-z.

[49] M. L. Seol *et al.*, “All 3D printed energy harvester for autonomous and sustainable resource utilization,” *Nano Energy*, vol. 52, no. July, pp. 271–278, 2018, doi: 10.1016/j.nanoen.2018.07.061.

[50] K. N. Kim, J. P. Lee, S.-H. Lee, S. C. Lee, and J. M. Baik, “Ergonomically designed replaceable and multifunctional triboelectric nanogenerator for a uniform contact,” *RSC Adv*, vol. 6, no. 91, pp. 88526–88530, Sep. 2016, doi: 10.1039/C6RA17429A.

[51] D. Jiang *et al.*, “A wearable noncontact free-rotating hybrid nanogenerator for self-powered electronics,” *InfoMat*, vol. 2, no. 6, pp. 1191–1200, Nov. 2020, doi: 10.1002/INF2.12103.

[52] S. A. Basith and A. Chandrasekhar, “COVID-19 clinical waste reuse: A triboelectric touch sensor for IoT-cloud supported smart hand sanitizer dispenser,” *Nano Energy*, vol. 108, Apr. 2023, doi: 10.1016/j.nanoen.2023.108183.

[53] M. Wajahat, A. Z. Kouzani, S. Y. Khoo, and M. A. P. Mahmud, “Comparative Study and Multi-Parameter Analysis to Optimize Device Structure of Triboelectric Nanogenerators,” *Nanotechnology*, Oct. 2023, doi: 10.1088/1361-6528/acd789.

[54] S. Liu, Y. Liu, Y. Chen, S. Wang, C. Men, and S. Gao, “Novel 3D Printed Vortex-like Flexible Roller-Compacted Triboelectric Nanogenerator for Self-Powered Electrochemical Degradation of Organic Contaminants,” *ACS Appl Mater Interfaces*, vol. 14, no. 15, pp. 17426–17433, 2022, doi: 10.1021/acsami.2c01750.

[55] D. Hong, Y. M. Choi, Y. Jang, and J. Jeong, “A multilayer thin-film screen-printed triboelectric nanogenerator,” *Int J Energy Res*, vol. 42, no. 11, pp. 3688–3695, 2018, doi: 10.1002/er.4092.

[56] M. A. P. Mahmud *et al.*, “3D-Printed Triboelectric Nanogenerators: State of the Art, Applications, and Challenges,” *Advanced Energy and Sustainability Research*, vol. 2, no. 3, p. 2000045, 2021, doi: 10.1002/aesr.202000045.

[57] Y. Chen *et al.*, “3D printed stretchable smart fibers and textiles for self-powered e-skin,” *Nano Energy*, vol. 84, p. 105866, Jun. 2021, doi: 10.1016/j.nanoen.2021.105866.

[58] M. Shahriar, C. P. Vo, and K. K. Ahn, “Self-powered Flexible PDMS Channel Assisted Discrete Liquid Column Motion Based Triboelectric Nanogenerator (DLC-TENG) as Mechanical Transducer,” *International Journal of Precision Engineering and Manufacturing - Green Technology*, vol. 6, no. 5, pp. 907–917, 2019, doi: 10.1007/s40684-019-00148-8.

[59] C. Wu *et al.*, “Electrohydrodynamic Jet Printing Driven by a Triboelectric Nanogenerator,” *Adv Funct Mater*, vol. 29, no. 22, pp. 1–8, 2019, doi: 10.1002/adfm.201901102.

[60] S. He *et al.*, “Polymer tubes as carrier boats of thermosetting and powder materials based on 3D printing for triboelectric nanogenerator with microstructure,” *Nano Energy*, vol. 52, no. July, pp. 134–141, 2018, doi: 10.1016/j.nanoen.2018.07.044.

[61] S. Chen *et al.*, “A Single Integrated 3D-Printing Process Customizes Elastic and Sustainable Triboelectric Nanogenerators for Wearable Electronics,” *Adv Funct Mater*, vol. 28, no. 46, p. 1805108, Nov. 2018, doi: 10.1002/adfm.201805108.

[62] S. Hasan, A. Z. Kouzani, S. Adams, J. Long, and M. A. P. Mahmud, “Comparative study on the contact-separation mode triboelectric nanogenerator,” *J Electrostat*, vol. 116, no. February, p. 103685, 2022, doi: 10.1016/j.elstat.2022.103685.

[63] X. Kang *et al.*, “Boosting performances of triboelectric nanogenerators by optimizing dielectric properties and thickness of electrification layer,” *RSC Adv*, vol. 10, no. 30, pp. 17752–17759, May 2020, doi: 10.1039/D0RA02181D.

[64] M. Kam, A. İpekçi, and Ö. Şengül, “Investigation of the effect of FDM process parameters on mechanical properties of 3D printed PA12 samples using Taguchi method,” *Journal of Thermoplastic Composite Materials*, vol. 36, no. 1, pp. 307–325, Jan. 2023, doi: 10.1177/08927057211006459.

[65] A. Salazar, A. Rico, J. Rodríguez, J. Segurado Escudero, R. Seltzer, and F. Martin De La Escalera Cutillas, “Monotonic loading and fatigue response of a bio-based polyamide PA11 and a petrol-based polyamide PA12 manufactured by selective laser sintering,” *Eur Polym J*, vol. 59, pp. 36–45, Oct. 2014, doi: 10.1016/J.EURPOLYMJ.2014.07.016.

[66] C. Cai *et al.*, “Comparative study on 3D printing of polyamide 12 by selective laser sintering and multi jet fusion,” *J Mater Process Technol*, vol. 288, no. August 2020, p. 116882, 2021, doi: 10.1016/j.jmatprotec.2020.116882.
[67] “VeroClear: A Transparent 3D Printing Material.” Accessed: Oct. 05, 2023. [Online]. Available: https://www.stratasys.com/en/materials/materials-catalog/polyjet-materials/veroclear/
[68] J. C. Santos, C. D. Almeida, A. Iwahara, and J. E. Peixoto, “Characterization and applicability of low-density materials for making 3D physical anthropomorphic breast phantoms,” *Radiation Physics and Chemistry*, vol. 164, p. 108361, Nov. 2019, doi: 10.1016/J.RADPHYSCHEM.2019.108361.
[69] A. Pugalendhi, R. Ranganathan, and S. Ganesan, “Impact of process parameters on mechanical behaviour in multi-material jetting,” *Mater Today Proc*, vol. 46, pp. 9139–9144, Jan. 2021, doi: 10.1016/J.MATPR.2019.12.106.
[70] D. K. Gupta, A. Tuli, and A. Jain, “3D printed material application in orthodontics,” *Mater Today Proc*, vol. 28, pp. 1635–1642, Jan. 2020, doi: 10.1016/J.MATPR.2020.04.856.
[71] G. Khandelwal, N. P. Maria Joseph Raj, and S. J. Kim, “Materials Beyond Conventional Triboelectric Series for Fabrication and Applications of Triboelectric Nanogenerators,” *Advanced Energy Materials*, vol. 11, no. 33. John Wiley and Sons Inc, Sep. 01, 2021. doi: 10.1002/aenm.202101170.
[72] H. Zou *et al.*, “Quantifying the triboelectric series,” *Nat Commun*, vol. 10, no. 1, Dec. 2019, doi: 10.1038/s41467-019-09461-x.
[73] H. Zou *et al.*, “Quantifying and understanding the triboelectric series of inorganic non-metallic materials,” *Nat Commun*, vol. 11, no. 1, Dec. 2020, doi: 10.1038/s41467-020-15926-1.
[74] HP Development Company, “HP 3D High Reusability PA 12 Glass Beads,” pp. 5–6, 2019.
[75] S. R. Begum and A. Chandrasekhar, “Opportunities and Challenges in Power Management Systems for Triboelectric Nanogenerators,” *ACS Applied Electronic Materials*, vol. 5, no. 3. American Chemical Society, pp. 1347–1375, Mar. 28, 2023. doi: 10.1021/acsaelm.2c01505.
[76] C. Tantardini and A. R. Oganov, “Thermochemical electronegativities of the elements,” *Nat Commun*, vol. 12, no. 1, Dec. 2021, doi: 10.1038/s41467-021-22429-0.
[77] J. W. Lee *et al.*, “Robust nanogenerators based on graft copolymers via control of dielectrics for remarkable output power enhancement,” *Sci Adv*, vol. 3, no. 5, 2017, doi: 10.1126/sciadv.1602902.
[78] D. W. Kim, J. H. Lee, J. K. Kim, and U. Jeong, “Material aspects of triboelectric energy generation and sensors,” *NPG Asia Mater*, vol. 12, no. 1, 2020, doi: 10.1038/s41427-019-0176-0.
[79] A. Touris *et al.*, “Effect of molecular weight and hydration on the tensile properties of polyamide 12,” *Results in Materials*, vol. 8, Dec. 2020, doi: 10.1016/j.rinma.2020.100149.
[80] G. S. Martynková *et al.*, “Polyamide 12 materials study of morpho-structural changes during laser sintering of 3d printing,” *Polymers (Basel)*, vol. 13, no. 5, Mar. 2021, doi: 10.3390/polym13050810.
[81] A. Ahmed *et al.*, “All printable snow-based triboelectric nanogenerator,” *Nano Energy*, vol. 60, pp. 17–25, Jun. 2019, doi: 10.1016/j.nanoen.2019.03.032.
[82] S. L. Zhang *et al.*, “Electromagnetic Pulse Powered by a Triboelectric Nanogenerator with Applications in Accurate Self-Powered Sensing and Security,” *Adv Mater Technol*, vol. 5, no. 10, p. 2000368, Oct. 2020, doi: 10.1002/admt.202000368.
[83] S. S. K. Mallineni, Y. Dong, H. Behlow, A. M. Rao, and R. Podila, “A Wireless Triboelectric Nanogenerator,” *Adv Energy Mater*, vol. 8, no. 10, pp. 1–7, 2018, doi: 10.1002/aenm.201702736.
[84] Q. Zhang, Z. Zhang, Q. Liang, Q. Shi, M. Zhu, and C. Lee, “All in One, Self-Powered Bionic Artificial Nerve Based on a Triboelectric Nanogenerator,” *Advanced Science*, vol. 8, no. 12, pp. 1–13, 2021, doi: 10.1002/advs.202004727.
[85] K. Chen *et al.*, “Dynamic Photomask-Assisted Direct Ink Writing Multimaterial for Multilevel Triboelectric Nanogenerator,” *Adv Funct Mater*, vol. 29, no. 33, pp. 1–9, 2019, doi: 10.1002/adfm.201903568.